A simplified model for linear and nonlinear processes in thermoacoustic prime movers. Part II. Nonlinear oscillations

H. Yuan, S. Karpov, and A. Prosperetti
Department of Mechanical Engineering, The Johns Hopkins University, Baltimore, Maryland 21218

The simplified quasi-one-dimensional model of thermoacoustic devices formulated in Part I [Watanabe *et al.*, J. Acoust. Soc. Am. **102**, 3484–3496 (1997)] is studied in the nonlinear regime. A suitable numerical method is described which is able to deal with the steep waveforms that develop in the system without inducing spurious oscillations, appreciable numerical damping, or numerical diffusion. The results are compared with some experimental ones available in the literature. Several of the observed phenomena are reproduced by the model. Quantitative agreement is also reasonable when allowance is made for likely temperature nonuniformities across the heat exchangers. © *1997 Acoustical Society of America.* [S0001-4966(97)01512-9]

INTRODUCTION

The literature contains evidence of the presence of nonlinear processes in thermoacoustic devices already at relatively low oscillation amplitudes (Atchley *et al.*, 1990a, 1990b). The available linear theory, although quite well developed (see, e.g., Rott, 1980; Wheatley, 1986; Swift, 1988), is incapable of dealing with these phenomena, nor does its extension into the nonlinear realm appear easy. Furthermore, even if such an attempt were successful, one would most likely end up with a very complex model that would not lend itself to the ready exploration of parameter space and the evaluation of different design alternatives.

These considerations motivated Part I of this study (Watanabe *et al.*, 1997), in which an approximate quasi-one-dimensional model of thermoacoustic devices was developed by integrating over the cross-sectional area. Although simplified, the model is nonlinear. Furthermore, upon linearization, it reproduces the pressure field and the eigenfrequencies of the linear theory exactly.

In the present paper we continue the analysis of the model extending it into the nonlinear regime. Our initial attempts in this direction (Prosperetti and Watanabe, 1994) encountered numerical difficulties due to the ready appearance of quasi-shock waves in the system. Overcoming this obstacle has required the adoption of a rather complex numerical method that is described in detail in Sec. III of this paper. In Sec. IV a comparison between the numerical results and some available experimental data is presented. Experimentally observed phenomena such as unstable growth of the wave and eventual saturation are well reproduced in qualitative terms. The computed wave amplitude tends to be higher than the measured one, probably due, among others, to an effectively lower temperature difference than the nominal value and to other dissipation phenomena not included in the model.

I. MODEL

We summarize here the equations of the present model. Their derivation can be found in Part I.

The equation of continuity is

$$\frac{\partial \rho}{\partial t} + \frac{1}{S} \frac{\partial}{\partial x} (S\rho u) = 0. \tag{1}$$

Here, x is the coordinate along the axis of the device (not necessarily rectilinear), $S(x)$ is the local cross sectional area, and ρ and u are the gas density and axial velocity averaged over the cross-sectional area. The momentum equation takes the form

$$\frac{\partial}{\partial t} (\rho u) + \frac{1}{S} \frac{\partial}{\partial x} (S\rho u^2) + \frac{\partial p}{\partial x} = -\mathscr{D}(u), \tag{2}$$

where p is the cross-sectional average of the gas pressure and the drag operator $\mathscr{D}$ will be specified shortly. The energy equation is used in the form

$$\frac{\partial}{\partial t} \left(\frac{1}{\gamma - 1} p + \frac{1}{2} \rho u^2 \right) + \frac{1}{S} \frac{\partial}{\partial x} \left[uS \left(\frac{\gamma}{\gamma - 1} p + \frac{1}{2} \rho u^2 \right) \right]$$
$$= \mathscr{H}(T_w - T) - \frac{dT_w}{dx} \mathscr{Q}(u), \tag{3}$$

where γ is the ratio of the specific heats of the gas, T the cross-sectional average of the gas temperature, $T_w(x)$ the surface temperature of the solid surfaces in contact with the gas, and the operators $\mathscr{H}$, $\mathscr{Q}$ will be specified below. In the present model, the temperature distribution T_w along the stack will be taken as given and independent of time. Work on an improved model in which this quantity is calculated is currently under way. The set of equations is closed by assuming the validity of the equation of state of perfect gases, namely,

$$p = R\rho T, \tag{4}$$

where R is the universal gas constant divided by the gas molecular mass.

A key aspect of the model is the specification of the terms $\mathscr{D}$, $\mathscr{H}$, and $\mathscr{Q}$. On the basis of the results of Part I we set

$$\mathscr{D}(u) = D\rho \left[1 + \theta_V \left(\frac{\partial}{\partial t} + u \frac{\partial}{\partial x} \right) \right] u, \tag{5}$$

$$\mathscr{H}(T_w - T) = H\rho c_p \left[1 + \theta_T\left(\frac{\partial}{\partial t} + u\frac{\partial}{\partial x}\right)\right](T_w - T)$$
$$+ k_n \frac{\partial^2}{\partial x^2}\left(\frac{1}{\gamma - 1}p + \frac{1}{2}\rho u^2\right), \qquad (6)$$

$$\mathscr{Q}(u) = c_p\rho Q\left[1 - \theta_Q\left(\frac{\partial}{\partial t} + u\frac{\partial}{\partial x}\right)\right]u, \qquad (7)$$

where c_p is the gas specific heat at constant pressure. In the version of the model presented in Part I the term with the second spatial derivative in (6) was omitted. It is introduced here for reasons discussed in the next section; the quantity k_n is a constant. In Part I the other parameters have been estimated by imposing that the results of the linear version of the model reproduce those of the exact linear theory. In this way it was determined that

$$D(1 + i\omega\theta_V) = i\omega\frac{f_V}{1 - f_V}, \qquad (8)$$

$$H(1 + i\omega\theta_T) = i\omega\frac{f_K}{1 - f_K}, \qquad (9)$$

$$Q(1 - i\omega\theta_Q) = \frac{1}{1 - \sigma}\left(\frac{1}{1 - f_V} - \frac{\sigma}{1 - f_K}\right) - 1, \qquad (10)$$

with σ the gas Prandtl number. For a stack consisting of plane parallel plates spaced by an amount l one has

$$f_V = \frac{\tanh(1 + i)l/2\delta_V}{(1 + i)l/2\delta_V}, \qquad (11)$$

where δ_V is the viscous boundary layer thickness given by

$$\delta_V = \sqrt{\frac{2\mu}{\omega\rho}}. \qquad (12)$$

Outside the stack region, l should be taken as the hydraulic diameter of the local cross section. The function f_K has the same expression (11) with δ_V replaced by the thermal boundary layer thickness $\delta_K = \delta_V/\sqrt{\sigma}$. Graphs of $if/(1-f)$ are given in Part I. Upon separating real and imaginary parts, the coefficients in the left-hand sides of (8)–(10) are readily determined.

If the parameter ω is chosen as one of the linear eigenmodes of the system, a linearization of the present model will reproduce the exact pressure eigenequation of the linear theory (Rott, 1976). In a nonlinear, time-dependent calculation, frequencies cannot be easily separated and a definite single value of ω must be committed to. We address this point in the next section.

For the present prime mover case, the velocity must vanish at the tube ends:

$$u = 0 \quad \text{at } x = 0, \quad x = L. \qquad (13)$$

The momentum equation (2) then implies that

$$\frac{\partial p}{\partial x} = 0 \quad \text{at } x = 0, \quad x = L. \qquad (14)$$

As shown in I, it follows from the energy and continuity equations that the temperature satisfies, at both ends,

$$\left[\frac{\partial}{\partial t} + H\left(1 + \theta_T\frac{\partial}{\partial t}\right)\right]T = \frac{\gamma - 1}{\gamma}\frac{T}{p}\frac{\partial p}{\partial t} + H\left(1 + \theta_T\frac{\partial}{\partial t}\right)T_w$$
$$+ \frac{k_n}{\gamma}\frac{T}{p}\frac{\partial^2 p}{\partial x^2}. \qquad (15)$$

We assume that $\partial T/\partial x = 0$ at the end points. Since the constant k_n will be taken to be very small and, away from the stack region, H is also very small, this relation then essentially implies the adiabatic pressure–temperature relation of perfect gases.

The velocity boundary condition (13) at $x = 0$ will be modified for the simulation of a piston-driven tube described later in Sec. IV.

II. THE LINEAR SPECTRUM

As shown in Part I if, in the expressions (5)–(7) for the momentum and energy transfer terms $\mathscr{D}$, $\mathscr{H}$, and $\mathscr{Q}$, ω is chosen as the exact eigenfrequency of any one mode, the linear version of the present model with $k_n = 0$ gives the pressure equation of the exact Rott theory for that mode [see Eq. (6) in Rott (1976) or Eq. (60) in Part I]. In a time-dependent nonlinear calculation as the one of present concern the separation of modes, although not impossible, is a nontrivial task that we have not attempted. For the purposes of this study we shall use a single value of ω that we denote by ω_0. While this will be treated as an adjustable parameter, it will always be close to the (real part of the) fundamental mode of the system for which an approximation can be given as

$$\bar{\omega} = \frac{\sqrt{\gamma R \bar{T}_w}}{L}, \qquad (16)$$

where $\bar{T}_w$ is the average wall temperature:

$$\bar{T}_w = \frac{1}{L}\int_0^L T_w(x)dx. \qquad (17)$$

The need to fix the parameter ω has a strong effect on the linear spectrum of the problem, that is reflected in the nonlinear calculations.

To illustrate this point, we show in Fig. 1 the imaginary part Im ω_n of the exact linear eigenvalues as a function of the mode number n, with $1 \leq n \leq 20$. The circles are connected by a solid line as an aid to the eye. The conditions here are as specified in Sec. IV below in connection with Fig. 7, but the general behavior is typical. The eigenvalue problem was solved by the inverse iteration method (Press et al., 1992). It is seen that only the first mode is unstable (Im $\omega_1 < 0$). The second one has a relatively small damping (with a Q value of approximately 170), and all the other ones are heavily damped. If one calculates the linear eigenvalues keeping ω_0 equal to $\bar{\omega} = 3327.7$ s^{-1}, instead, the results shown by the triangles and the dashed line are found. Although the first few eigenvalues are not very different, the approximation renders several of the higher-order modes unstable as well. The consequence of this is that, while a numerical calculation with a coarse discretization (and a consequently large numerical damping) would superficially look acceptable, an
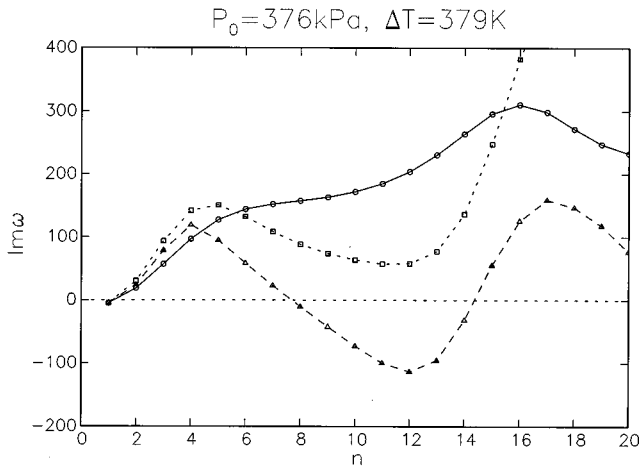
FIG. 1. Imaginary part of the first 20 eigenvalues for the system and conditions of Fig. 7 below. The circles connected by the solid line are the exact results of the linear theory. Note that only the first mode is unstable (Im $\omega_1 < 0$). The results shown by the triangles and the dashed line correspond to setting the parameter ω in Eqs. (5)–(7) equal to $\bar{\omega}$ defined in (16) that here has the value 3327.7 s^{-1}. The higher modes become unstable with this approximation. The squares and the dotted line are the linear spectrum for $\omega = \omega_0 = 2762.0$ s^{-1} and $k_n = 0.25$ m^2/s.
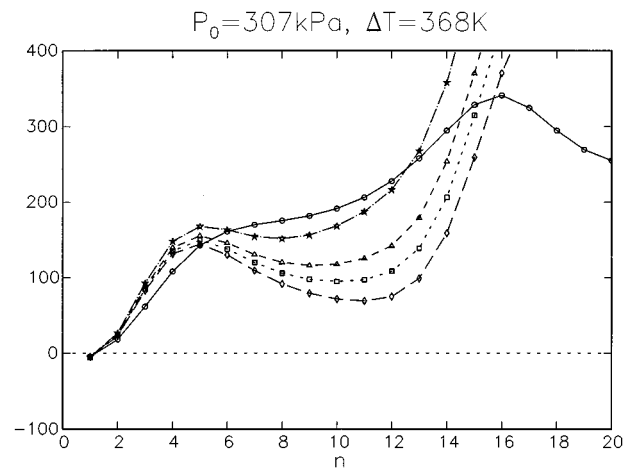

FIG. 2. (a) Imaginary part of the first 20 eigenvalues for the system and conditions of Fig. 8 below. The circles connected by the solid line are the exact results of the linear theory. The other lines, in descending order, correspond to $\omega_0 = 2658.6$ s^{-1}, $k_n = 0.42$ m^2/s, $\omega_0 = 2791.5$ s^{-1}, $k_n = 0.31$ m^2/s, $\omega_0 = 2858.0$ s^{-1}, $k_n = 0.26$ m^2/s, $\omega_0 = 2924.4$ s^{-1}, $k_n = 0.21$ m^2/s.

attempt to refine the grid would lead to the rapid growth of short-wavelength instabilities that destroy the calculation. The thermoacoustic effect requires a very delicate balance and does not easily survive approximations.

This is the reason why we have introduced a second-derivative in the exchange term $\mathcal{H}$. With a suitable adjustment of ω_0 and of the "pseudo-thermal conductivity" k_n, we can approximate the important first few linear modes and dampen the higher ones. As an example we show (dotted line, squares) the effect of choosing $\omega_0 = 2762.0$ s^{-1} and $k_n = 0.25$ m^2/s. It is seen that the only large differences between the exact and the approximate results are relegated to the high-order modes that are heavily damped anyway and should therefore not have a large effect on the results. It might appear that treating both ω_0 and k_n as adjustable parameters makes the formulation of the model nonunique. In practice, however, we find that the two requirements of matching the growth rate of the unstable mode and requiring the higher modes to be all damped leaves little room to adjust the values of these two quantities. In particular, as will be seen in Sec. IV, the nonlinear steady-state amplitudes are not greatly affected.

Figure 2 is similar to Fig. 1 and shows some examples for the case of Fig. 8 below. The circles and the solid line are again the exact spectrum, for which Im $\omega_1 = -4.73$ s^{-1}. The other lines, in descending order, correspond to $\omega_0 = 2658.6$ s^{-1}, $k_n = 0.42$ m^2/s (Im $\omega_1 = -4.71$ s^{-1}), $\omega_0 = 2791.5$ s^{-1}, $k_n = 0.31$ m^2/s (Im $\omega_1 = -4.73$ s^{-1}), $\omega_0 = 2858.0$ s^{-1}, $k_n = 0.26$ m^2/s (Im $\omega_1 = -4.72$ s^{-1}), $\omega_0 = 2924.4$ s^{-1}, $k_n = 0.21$ m^2/s (Im $\omega_1 = -4.72$ s^{-1}). All these curves differ by very little for the first few modes which carry most of the energy. The main differences are in the higher modes, which have a minor effect on the waveform of the steady-state solution as will be seen in Sec. IV.

In principle, one can avoid the approximations just de-

scribed by calculating the exchange terms by means of convolutions in time with kernels given by the inverse Fourier transforms of (8)–(10). This procedure would, however, add further complexity to the calculation. Another approximate scheme, possibly better than the one used here, could be to specify the exchange terms by means of differential equations rather than explicitly as done above. This approach has been advocated by Achard and Lespinard (1981) for the similar problem of the time-dependent flow in a tube.

We plan to pursue this idea in future work. For the time being we proceed in the manner described. Even though this is an approximation, it enables us to gain some insight into the time-dependent problem, nonlinear growth, and eventual saturation, for which no theoretical framework is currently available.

III. NUMERICAL METHOD

With the expressions (5)–(7), and the definitions

$$m = \rho u, \quad e = \frac{1}{\gamma - 1} p + \frac{1}{2} \rho u^2, \tag{18}$$

for the momentum flux m and total energy e it is easy to verify that the continuity, momentum, and energy equations (1), (2), and (3) may equivalently be written as

$$\frac{\partial \rho}{\partial t} + \frac{\partial m}{\partial x} + \frac{m}{S} \frac{\partial S}{\partial x} = 0, \tag{19}$$

$$\frac{\partial m}{\partial t} + \frac{\partial}{\partial x} (mu + p) + \frac{mu}{S} \frac{\partial S}{\partial x}$$

$$= 0 = -D \left[m + \theta_V \left(\frac{\partial m}{\partial t} + \frac{1}{S} \frac{\partial}{\partial x} (muS) \right) \right], \tag{20}$$

$$\frac{\partial e}{\partial t}+\frac{\partial}{\partial x}[u(e+p)]+\frac{u}{S}(e+p)\frac{\partial S}{\partial x}$$

$$=Hc_p\rho(T_w-T)-\gamma H\theta_T\left[\frac{\partial e}{\partial t}+\frac{\partial}{\partial x}(ue)-u\frac{\partial m}{\partial t}-\frac{1}{2}u^2\right.$$

$$\times\frac{\partial\rho}{\partial t}-\frac{1}{2}\frac{\partial}{\partial x}(mu^2)\bigg]-m\frac{dT_w}{dx}c_p(H\theta_T+Q)$$

$$+\frac{dT_w}{dx}c_pQ\theta_Q\left[\frac{\partial m}{\partial t}+\frac{\partial}{\partial x}(um)\right]+k_n\frac{\partial^2 e}{\partial x^2}. \tag{21}$$

We rewrite this system of equations in vector form as

$$\frac{\partial\mathbf{w}}{\partial t}+\frac{\partial\mathbf{F}}{\partial x}+\mathbf{s}=\mathbf{B}\frac{\partial\mathbf{w}}{\partial t}+\mathbf{b}, \tag{22}$$

where $\mathbf{w}$ is given by

$$\mathbf{w}=\begin{vmatrix}\rho\\m\\e\end{vmatrix}, \tag{23}$$

the flux vector $\mathbf{F}$ by

$$\mathbf{F}=\begin{vmatrix}\rho u\\\rho u^2+p\\(e+p)u\end{vmatrix} \tag{24}$$

the vector $\mathbf{s}$ accounting for the effect of changes in the cross-sectional area by

$$\mathbf{s}=\begin{vmatrix}\rho u\\\rho u^2\\(e+p)u\end{vmatrix}\frac{1}{S}\frac{\partial S}{\partial x}, \tag{25}$$

and

$$\mathbf{B}=\begin{vmatrix}0 & 0 & 0\\0 & -D\theta_V & 0\\H\theta_T\left(c_pT_w-\frac{1}{2}\gamma u^2\right) & \gamma H\theta_T u+\frac{dT_w}{dx}c_pQ\theta_Q & -\gamma H\theta_T\end{vmatrix}, \tag{26}$$

$$\mathbf{b}=\begin{vmatrix}0\\-D\left[m+\frac{\theta_V}{S}\frac{\partial}{\partial x}(Sum)\right]\\Hc_p\left[\rho(T_w-T)+\frac{\theta_T}{S}\frac{\partial}{\partial x}[\rho uS(T_w-T)]\right]-\frac{dT_w}{dx}c_pQ\left[m-\frac{\theta_Q}{S}\frac{\partial}{\partial x}(umS)+k_n\frac{\partial^2 e}{\partial x^2}\right]\end{vmatrix}. \tag{27}$$

Our first attempt at solving Eq. (22) was based on a straightforward centered-difference spatial discretization with a predictor–corrector time stepping procedure (Prosperetti and Watanabe, 1994). We found that, whenever conditions were such that quasi-shocks developed, a series of spurious grid-dependent oscillations also appeared. Such oscillations are a well-known numerical artifact affecting computations in the presence of steep gradients (see, e.g., Roe, 1986; Fletcher, 1988), and their elimination has motivated a large amount of research. While a complete bibliography would be out of place here, it may be useful to cite the review by Roe (1986) and a few other papers (Sod, 1978; Harten, 1983; Osher, 1984; Osher and Chakravarthy, 1984; Sweby, 1984; Harten *et al.*, 1986; Harten and Osher, 1987). This effort has led to a new family of schemes for hyperbolic equations known as total variation diminishing (TVD) schemes. The name is a consequence of the definition of the *total variation* $\mathrm{TV}(u^n)$ of a grid function $\{u_i^n\}$, $i=1,2,...,$ $N+1$ at time t^n:

$$\mathrm{TV}(u^n)=\sum_{i=1}^{N}|u_{i+1}^n-u_i^n|, \tag{28}$$

and of the fact that these schemes have the property that $\mathrm{TV}(u^n)$ is a nonincreasing function of time:

$$\mathrm{TV}(u^n)\geqslant\mathrm{TV}(u^{n+1}). \tag{29}$$

Evidently, a TVD scheme cannot produce an oscillatory solution starting from monotonic initial data. We have found that the scheme proposed by Harten (1983) proved suitable for our problem.

The system (22) is first discretized explicitly in time as

$$(\mathbf{I}-\mathbf{B}_i^n)\frac{\mathbf{w}_i^{n+1}-\mathbf{w}_i^n}{\Delta t}+\frac{\hat{\mathbf{F}}_{i+1/2}^n-\hat{\mathbf{F}}_{i-1/2}^n}{\Delta x}+\mathbf{s}_i^n=\mathbf{b}_i^n, \tag{30}$$

where superscripts indicate time levels and subscripts spatial nodes. The spatial derivatives appearing in $\mathbf{B}$ and $\mathbf{s}$ are discretized by central differences. The essential aspect of the numerical method is the manner in which the modified fluxes $\hat{\mathbf{F}}$ are specified in terms of some auxiliary quantities that we now define.

Let

$$\mathbf{R}^{(1)}=\begin{vmatrix}1\\u-c\\\frac{e+p}{\rho}-uc\end{vmatrix},\quad\mathbf{R}^{(2)}=\begin{vmatrix}1\\u\\\frac{1}{2}u^2\end{vmatrix},$$

$$\mathbf{R}^{(3)}=\begin{vmatrix}1\\u+c\\\frac{e+p}{\rho}+uc\end{vmatrix}. \tag{31}$$

where $c=\sqrt{\gamma RT}$, and

$$a^{(1)} = u - c, \quad a^{(2)} = u, \quad a^{(3)} = u + c. \qquad (32)$$

Furthermore, let

$$\alpha_i^{(1)} = \frac{1}{2c_{i+1/2}^2} \left[(p_{i+1} - p_i) - \rho_{i+1/2} c_{i+1/2}(u_{i+1} - u_i) \right.$$

$$\left. + \frac{\rho_{i+1/2} u_{i+1/2} c_{i+1/2}^2}{(u_{i+1/2} - c_{i+1/2}) S_{i+1/2}} (S_{i+1} - S_i) \right], \qquad (33)$$

$$\alpha_i^{(2)} = \frac{1}{c_{i+1/2}^2} \left[c_{i+1/2}^2 (\rho_{i+1} - \rho_i) - (p_{i+1} - p_i) \right], \qquad (34)$$

$$\alpha_i^{(3)} = \frac{1}{2c_{i+1/2}^2} \left[(p_{i+1} - p_i) + \rho_{i+1/2} c_{i+1/2}(u_{i+1} - u_i) \right.$$

$$\left. + \frac{\rho_{i+1/2} u_{i+1/2} c_{i+1/2}^2}{(u_{i+1/2} + c_{i+1/2}) S_{i+1/2}} (S_{i+1} - S_i) \right], \qquad (35)$$

where the quantities carrying a half-integer subscript are calculated as arithmetic averages, e.g., $u_{i+1/2} = 1/2(u_{i+1} + u_i)$. Then

$$\hat{\mathbf{F}}_{i+1/2} = \frac{1}{2}(\mathbf{F}_{i+1} + \mathbf{F}_i) + \frac{\Delta t}{2\Delta x} \sum_{l=1}^{3} [g_i^{(l)} + g_{i+1}^{(l)} - Q(\nu_{i+1/2}^{(l)}$$

$$+ \gamma_i^{(l)}) \alpha_i^{(l)}] \mathbf{R}_{i+1/2}^{(l)}, \qquad (36)$$

where

$$\nu^{(l)} = \frac{\Delta t}{\Delta x} a^{(l)}, \quad \gamma_i^{(l)} = \frac{g_{i+1}^{(l)} - g_i^{(l)}}{\alpha_i^{(l)}}. \qquad (37)$$

The quantities $g_i^{(l)}$ appearing in these definitions are a correction to the components of the flux $\mathbf{F}$ along the characteristic directions and are the smaller one in modulus between

$$[Q(\nu_{i+1/2}^{(l)}) - \nu_{i+1/2}^{(l)}] \alpha_{i+1/2}^{(l)},$$

and $\qquad\qquad\qquad\qquad\qquad\qquad\qquad\qquad (38)$

$$[Q(\nu_{i-1/2}^{(l)}) - \nu_{i-1/2}^{(l)}] \alpha_{i-1/2}^{(l)}.$$

This flux correction is introduced to account for the discretization error and guarantees second-order accuracy in space.

The last quantity to be defined is the function $Q(x)$ that may be considered as a modified $|x|$. Specifically, following Harten (1983), we take

$$Q(x) = \frac{x^2}{4\epsilon} + \epsilon, \quad \text{for } |x| < 2\epsilon,$$

$$= |x|, \quad \text{for } |x| \geq 2\epsilon, \qquad (39)$$

with $\epsilon = 0.1$. This quantity plays the role of an artificial viscosity.

Since the integration is explicit in time, the preceding formulas are sufficient to construct the solution at all the interior nodes at time level t^{n+1} starting from the known values at t^n. The solution at the two boundary nodes is calculated from the boundary conditions (13)–(15).

IV. RESULTS

As a first test of the numerical method, we consider the thermoviscous damping of the lowest linear acoustic mode in a rigid-walled, empty, isothermal tube. Since an exact solu-
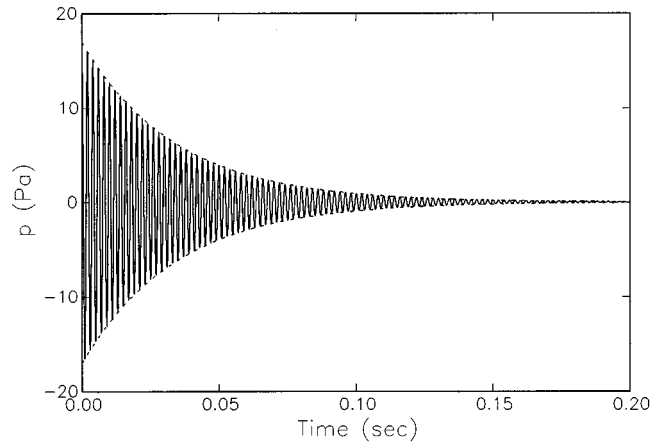

FIG. 3. Decay of pressure oscillations in a rigid isothermal tube for the conditions described in the text. The solid line is the result of the numerical computation. The dashed lines are the exponential envelope proportional to $\pm \exp(-bt)$ with b given by (40).

tion to this problem is available, this simulation is a useful test of the numerical method. Theoretically the solution consists of exponentially damped oscillations with a decay rate b given by (see, e.g., Pierce, 1989, p. 534; the spatial decay rate given in this text can be converted to a temporal one by dividing by the sound speed $c = \sqrt{\gamma R T_w}$):

$$b = \frac{c}{2a\gamma} \left[(\gamma - 1) \frac{\omega_0 \sigma k}{2 p_0 R} \right]^{1/2} \left(1 + \frac{\gamma - 1}{\sqrt{\sigma}} \right), \qquad (40)$$

where a is the tube radius, k the gas thermal conductivity, p_0 the undisturbed pressure, and $\omega_0 = \pi c/L$ the natural frequency of the eigenmode.

The pressure at one of the tube's rigid terminations given by the numerical method described in the previous section is shown in Fig. 3 as a function of time. The tube has a length of 99.9 cm and a diameter of 3.82 cm. The gas is helium at a static pressure $p_0 = 170$ kPa and temperature $T_w = 293$ K. For this case there are no unstable modes and we set $k_n = 0$ in Eqs. (8) and (9) and fix ω as in Eq. (16).

At time 0 the system is at rest with an initial pressure disturbance consisting of the lowest eigenmode with an amplitude of 17 Pa. The dashed lines in Fig. 3 are the exponential envelope $\propto \exp(-bt)$ with b given by (40). The agreement between the analytical and numerical results is remarkably good, which gives some confidence on our computer code. For these calculation 500 nodes proved sufficient for a good resolution and the time step was adjusted so that the maximum Courant number $\Delta t |a^{(i)}|/\Delta x$, with the $a^{(i)}$ defined in Eq. (32), remained below 0.8.

As another test, we consider the nonlinearly driven tube studied by Gaitan and Atchley (1993). The tube contained air at ambient pressure and temperature and was 82.55 cm long with a diameter of 5.82 cm. For this simulation we excite the tube by prescribing a sinusoidal gas velocity at $x = 0$. The boundary conditions on pressure and temperature are still given by (14) and (15). Again there are no unstable modes and we set $k_n = 0$.

In the experiment the driving frequency was chosen so as to match the pipe's frequency. We found that by using the
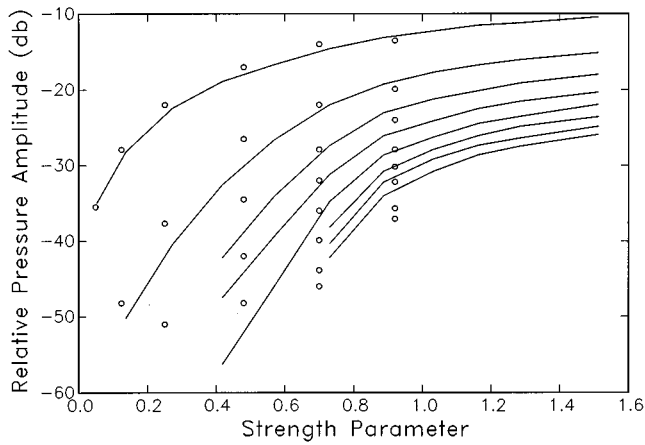
FIG. 4. Level of the harmonics of order 2–8 of a tube driven at resonance by a piston as a function of the level of the fundamental normalized according to (41). The lines are the present computational results. The data the experimental points of Gaitan and Atchley (1993).
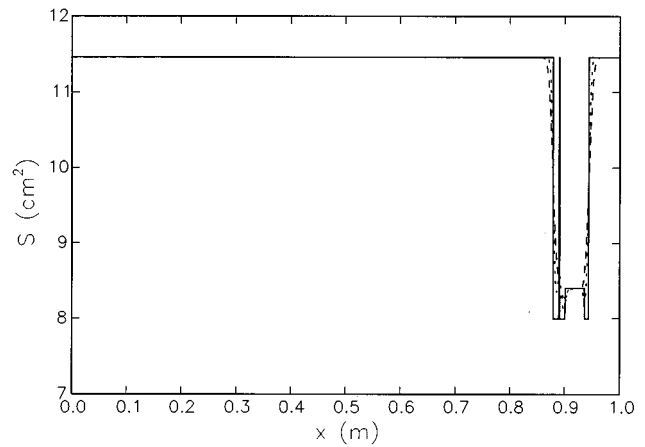
FIG. 5. The solid line is the cross-sectional area of the thermoacoustic prime mover of Atchley *et al.* (1992) and Atchley (1994) according to the geometrical specifications given in the papers. The dotted and dashed lines are the cross-sectional area after applying the smoothing operation of Part I 100 and 310 times, respectively.

reported value $f = 209$ Hz, our ''numerical pipe'' was not in exact resonance conditions. To match the resonance it was necessary to use $f = 207$ Hz. This sensitivity is not surprising in view of the rather large Q value of this system that, on the basis of our numerical results, is approximately 134. Gaitan and Atchley (1994) show in their Fig. 4 the dependence of the higher harmonic pressure amplitudes on the strength parameter, i.e., the amplitude P_1 of the fundamental normalized by

$$P_1^* = \frac{\beta Q}{\gamma p_0} P_1, \tag{41}$$

where β is the nonlinearity parameter equal to 1.2 for air. They do not report a value for Q and we used the one deduced from our computations quoted above. A comparison of the calculated (lines) and measured (circles) results is shown in Fig. 4. The comparison is very good especially for the lower harmonics that have a higher level and are therefore less sensitive to noise and parasitic damping. For these calculations we used 500 nodes and a maximum Courant number of 0.4.

We now turn to thermoacoustic prime movers, specifically the helium system used in the experiments of Atchley *et al.* (1992) and Atchley (1994). As described in these references, the tube length was 99.89 cm and the diameter 3.82 cm. The cold portion of the tube was 87.5 cm long. At the end of this section was the cold heat exchanger consisting of two identical structures separated by 1.5 mm. Each structure consisted of 25 nickel plates 0.45-mm thick, spaced by 1.04 mm and 1.02 cm long. Attached to the second part of the cold heat exchanger was the stack consisting of 3.5-cm-long stainless-steel plates spaced by 0.77 mm, with a thickness of 0.28 mm. The hot heat exchanger was attached to the other end of the stack. This heat exchanger was equal to the cold one except that it consisted of only one section 7.62 mm long. The hot section of the tube was 5.5 cm long. The area blockage fraction was approximately 30% in the heat exchangers and 27% in the stack.

We have pointed out in Part I the effect on the linear growth rate of the instability of using discontinuous versus smoothed prescriptions for the axial variation of the cross-sectional area and of the wall temperature. The discontinuities in area and axial derivative of the wall temperature are certainly not a realistic approximation to the actual spatial distribution of these parameters and their presence depends on features (such as natural convection, microstreaming, etc.) that are not included in the model. In Part I we have used a smoothing prescription

$$T_w(x_i) \rightarrow \tfrac{1}{4}[T_w(x_{i-1}) + 2T_w(x_i) + T_w(x_{i+1})] \tag{42}$$

(where x_i is the ith spatial node) iterated a number of times so as to have results in agreement with reported data, and we follow the same approach here. From the data reported by Atchley (1994) for a mean pressure of 376 kPa and a temperature difference of 379 K along the stack (and, presumably, an ambient temperature of 293 K), one finds that the temporal growth rate of the perturbation is 5.0 s^{-1}. Upon assuming discontinuous distributions for $S(x)$ and $T_w(x)$ we find from the exact linear theory 11.7 s^{-1}. By repeating the smoothing operation 310 times, the calculated linear growth rate becomes 5.13 s^{-1}. The cross-sectional area and wall temperature distributions resulting from smoothing 100 and 310 times are shown in Figs. 5 and 6. The corresponding initial unsmoothed distributions are shown by the solid lines. The difference is not large, which gives an indication of the sensitivity of the thermoacoustic energy conversion process. In all the calculations shown in this section we have used area and temperature distributions smoothed 310 times.

After matching the linear growth rate with the exact linear theory, in order to proceed with the time-dependent nonlinear calculation, we must select values of the parameter ω_0 and pseudoconductivity k_n. By a process of trial and error we find that, with $k_n = 0.25 \text{ m}^s/\text{s}$ and $\omega_0 = 2762.0 \text{ s}^{-1}$, the linear growth rate becomes 5.01 s^{-1} to be compared with the measured one of 5.0 s^{-1}. On the basis of a convergence
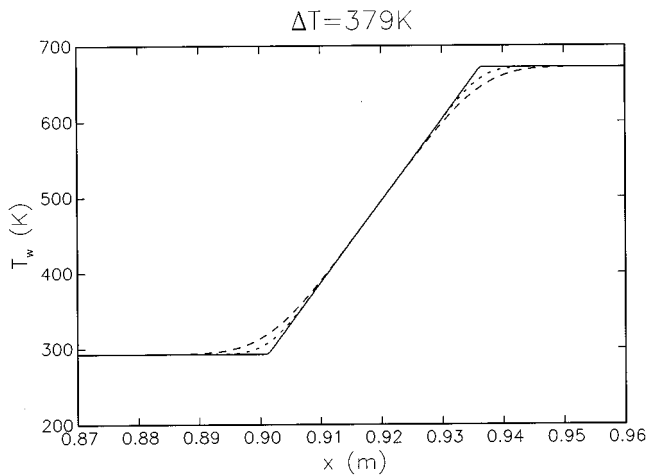
FIG. 6. Unsmoothed (solid line) and smoothed temperature distributions for the simulation of the case studied by Atchley (1994) and shown in Fig. 7. The dotted and dashed lines are the distributions after applying the smoothing operation of Part I 100 and 310 times, respectively.

study we found that 2000 spatial nodes are sufficient for a grid-independent solution. The maximum Courant number allowed was 0.4.

Figure 7 shows the numerically computed pressure at the cold end of the tube versus time for these conditions. The initial disturbance is taken to be the fundamental linear eigenmode, with an amplitude of 100 Pa. The dashed lines are graphs of an exponential growth with the growth rate of 5.13 s^{-1} of the exact linear theory. Figure 7(a) shows the initial buildup of the oscillations. The initial growth rate as deduced from these results is exponential, but at a rate of 5.25 s^{-1}, just slightly higher than the exact linear result of 5.13 s^{-1}. We consider this 2.3% difference as an acceptable consequence of the numerical error affecting the time-dependent calculation. At first the numerical results track with great precision the exponential growth. Soon thereafter, however, nonlinear effects set in as evidenced by the growing asymmetry between positive and negative pressure peaks. Figure 7(b) (note the change in the vertical scale) shows the same results over a longer time interval. Here one sees the eventual divergence of the linear result as opposed to the finite-amplitude stabilization of the nonlinear one.

Figure 7(b) shows that the system saturates at a positive pressure amplitude of approximately 25.0 kPa, i.e., about 6.6% of the static pressure. If the same calculation is repeated with cross-sectional area and wall temperature distributions smoothed only eight times instead of 301 (i.e., very nearly discontinuous), the saturation value for the positive pressure amplitude is approximately 41.0 kPa. Again, this is an indication of the sensitivity of the process.

We have found two papers in the literature where data are presented for nonlinear steady oscillations. One is by Atchley *et al.* (1990), and the other by Swift (1992). The stack used by the latter was of the honeycomb, rather than parallel plate, type and therefore cannot be simulated in the framework of the present model. Hence we focus on the results of Atchley *et al.*, and in particular on those corresponding to a nominal temperature difference along the stack of 368 °C that are documented in good detail in their paper.
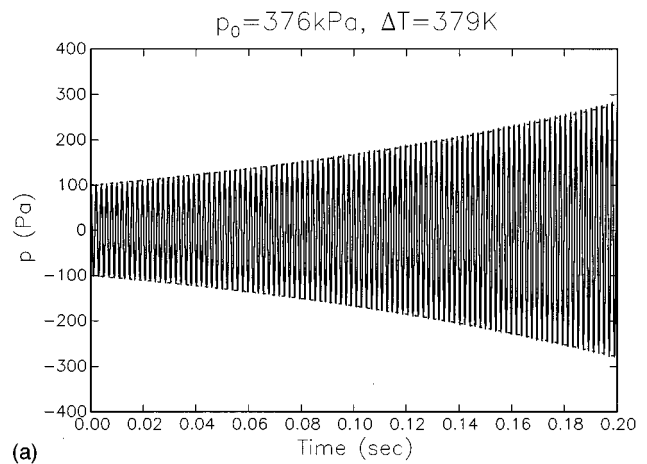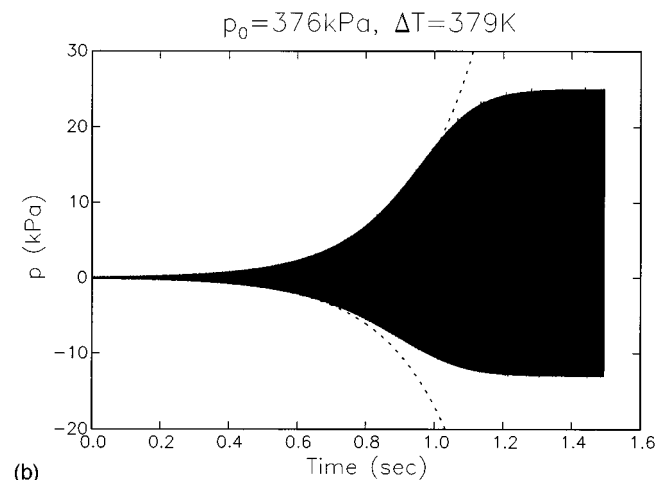
FIG. 7. Pressure versus time at the cold end of the prime mover for the case studied by Atchley (1994) described in the text. (a) shows the initial buildup of the oscillations, (b) shows the long-term evolution of the system to steady state. The dashed lines portray an exponential growth with the growth rate of 5.13 s^{-1} of the exact linear theory.

The experimental setup used in this work was the same described before in connection with Fig. 7.

Figure 8 shows the computed steady-state pressure disturbance at the cold end of the tube for a mean pressure of 307 kPa and a temperature difference along the stack $\Delta T = 368$ K. The solid line is for $\omega_0 = 2658.6 \text{ s}^{-1}$, $k_n = 0.42 \text{ m}^2/\text{s}$ and the dashed line for $\omega_0 = 2924.4 \text{ s}^{-1}$, $k_n = 0.21 \text{ m}^2/\text{s}$. The corresponding linear spectra are shown by the curves marked with stars and diamonds, respectively, in Fig. 2. The two waveforms are very similar to each other, in particular for what concerns the period and the amplitudes of the positive and negative portions. The main difference is the greater amount of fine structure present in the dashed curve that reflects the weaker attenuation of the higher modes evident from Fig. 2. The corresponding spectra are shown in Fig. 9, where also one observes mainly differences in the high-frequency components.

These results should be compared with those shown in Figs. 4 and 5 of Atchley *et al.* (1990). Qualitatively, the numerical results are close to the experimental ones. The period, 1.95 ms, is identical within the precision with which it can be read from the figure. The waveform exhibits a strong
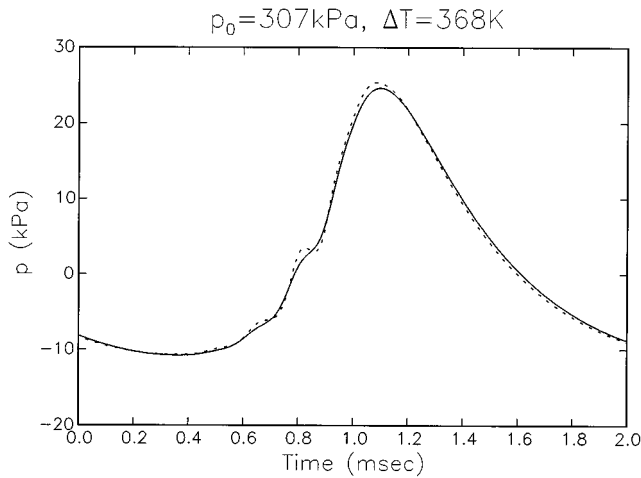
FIG. 8. Steady pressure waveform for a temperature difference between the hot and cold ends of the stack $\Delta T = 368$ K and the conditions of the experiment of Atchley *et al.* (1990) described in the text. The solid line is for $\omega_0 = 2658.6$ s^{-1}, $k_n = 0.42$ m^2/s, the dashed line for $\omega_0 = 2924.4$ s^{-1}, $k_n = 0.21$ m^2/s. The corresponding linear spectra are shown, respectively, by the stars and the diamonds in Fig. 2.

(a)

(b)

FIG. 9. Spectra of the pressure waveforms of the previous figure; (a) is for $\omega_0 = 2658.6$ s^{-1}, $k_n = 0.42$ m^2/s, (b) for $\omega_0 = 2924.4$ s^{-1}, $k_n = 0.21$ m^2/s. The corresponding linear spectra are shown, respectively, by the stars and the diamonds in Fig. 2.

asymmetry, with the negative amplitude much smaller than the positive one. The general spectral shapes also compare favorably with the spectrum flattening out 35–40 dB below the fundamental around the 6th to 7th harmonic. The major difference between calculations and experiment is the amplitude, that is about 24.7 kPa according to Fig. 8, but 13.5 kPa in the data.

Atchley (private communication) has pointed out to us that his temperature data were obtained from a thermocouple near the outer wall of the tube and, at such high power, a substantial temperature nonuniformity across the hot stack could be expected, as large as 50 K, with a likely value of 20–30 K. The present model is below the instability threshold if ΔT is reduced by 50 K. The result for a reduction of 25 K is shown in Fig. 10. Now the maximum pressure disturbance is 14.6 kPa, with the period (1.97 ms) hardly affected. However, the waveform shown in Fig. 10 exhibits a front less steep than the experimental one.

Other features of the results that can be compared with experiment are the ratio of the positive and negative amplitude, and the time interval between the zero crossings, e.g., of the positive part of the wave. The data for these quantities are 1.53 and 0.77 ms. (The latter quantity may, however, be affected by the fact that the experimental waveform exhibits some dc bias as the net area under the curve does not seem to vanish.) For the two computations of Fig. 8 the positive/negative ratio is 2.29 and 2.37, while the interval between zero crossings is 0.82 ms. For the smaller ΔT case of Fig. 10, the corresponding values are 1.97 and 0.90 ms.

Clearly, there are discrepancies between data and theory. Unfortunately, on the basis of the available information it is not clear whether the origin of the observed differences resides in the approximations of the present model or in the data. More detailed experiments would be highly desirable to help resolve the matter.

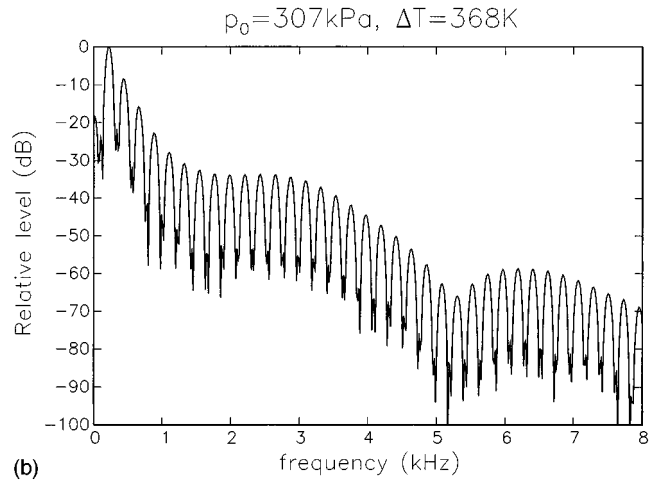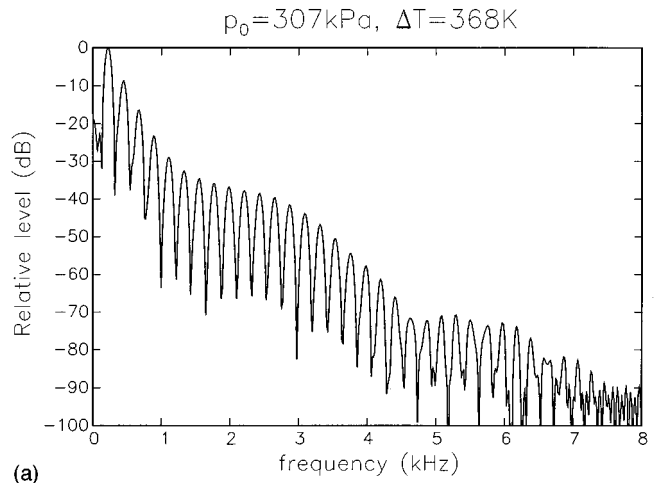Atchley *et al.* (1990) also report results for a smaller temperature gradient, with $\Delta T = 325$ K. In our model this is just below threshold, with Im $\omega_1 = 0.44$ s^{-1}. In view of the extreme sensitivity of a system so close to threshold to even minute adjustments of parameters or operating conditions, we do not feel that a comparison with these data would be meaningful.

As a last topic we give two examples that illustrate the effect of the tube's cross-sectional area distribution. The conditions and the system simulated are the same as in Fig. 8 except that the cross-sectional area of the midsection of the tube, for $\frac{1}{2}L < x < \frac{3}{4}L$, is given by

$$S(x) = S_0 \left[1 + C \, \cos^2 \, \pi \left(\frac{2x}{L} - 1 \right) \right]^2,$$

$$\text{for } \tfrac{1}{4}L \leqslant x \leqslant \tfrac{3}{4}L. \tag{43}$$

while $S = S_0 = \frac{1}{4}\pi(3.82)^2$ cm^2 elsewhere (except for the stack region). Figure 11 shows the steady-state pressure distribution at the cold end of the tube for $C = 0.2$. The pressure amplitude is now about five times that found for the constant-area case. The formation of a shock is also evident from the figure. If the tube is narrower in its central region,
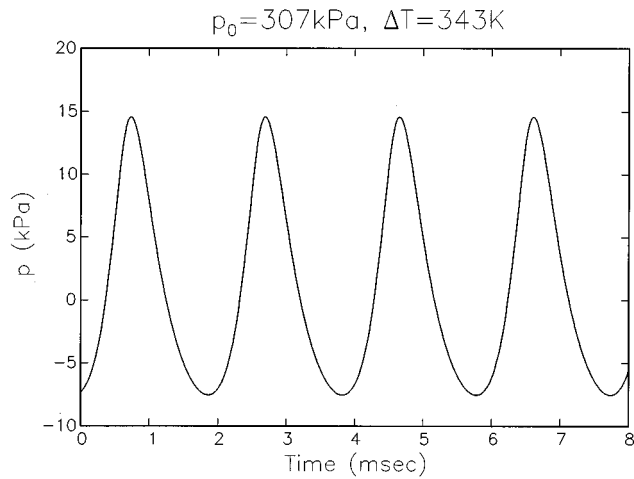
FIG. 10. Steady pressure waveform for $\Delta T = 343$ K and the other conditions as in Fig. 8. Time in ms.

on the other hand, we have the result shown in Fig. 12 for $C = -0.2$. The amplitude of the wave is now reduced by about 3% to approximately 24.4 kPa with respect to the constant area case. While the amplitude is not much different, the waveform is strongly affected with a markedly smaller steepening. These results are consistent with the corresponding linear ones presented in Part I.

V. CONCLUSIONS

In this paper we have adapted the model introduced in Part I to the nonlinear regime and we have described a reliable numerical method for its integration. The numerical results agree very well with experiment for the case of a resonantly driven tube. For a thermoacoustic prime mover, the model has been shown to describe the growth and eventual saturation of the oscillations. While the qualitative predictions match observation, the computed wave amplitude for a case studied by Atchley *et al.* (1990) exceeds the experimentally reported one. It does not seem possible to reach definite
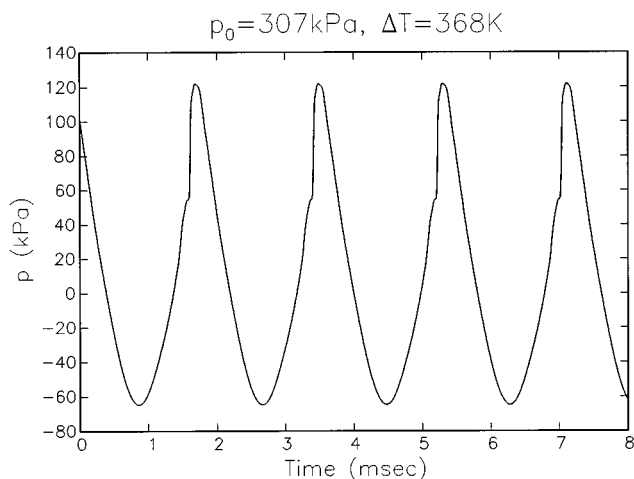

FIG. 11. Steady pressure waveform for the same conditions as in Fig. 8, except that the tube's cross section is enlarged in the midsection according to (43) with $C = 0.2$. Time in ms.
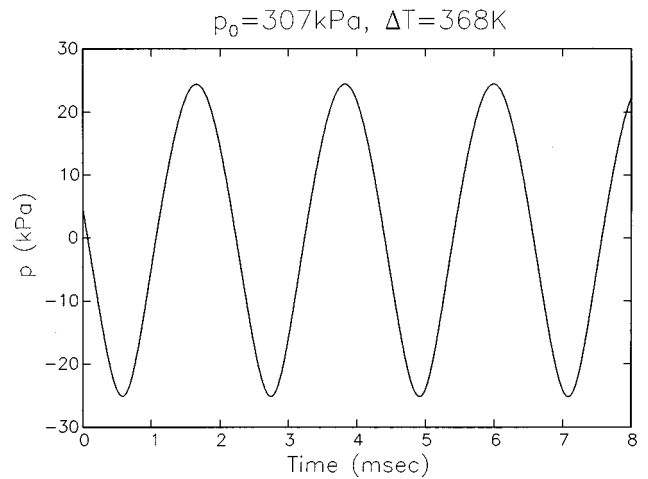

FIG. 12. Steady pressure waveform for the same conditions as in Fig. 8, except that the tube's cross section is decreased in the midsection according to (43) with $C = -0.2$. Time in ms.

conclusions on the reason for this discrepancy at this time. It is possible that in the experiment the actual temperature difference along the stack was less than the nominal value. It would also appear from the reported experimental waveform (Fig. 4 of Atchley *et al.*) that the mean of the pressure over the wave is not zero. We have also found that the simulation of this case is very sensitive to details of the temperature and cross-sectional area distribution. Lastly, the model requires the introduction of a certain number of approximations concerning critical terms that govern the energy exchange between the stack and the wave, and it is possible that the results are negatively affected by these approximations.

A more detailed characterization of future experiments would be desirable to resolve some of these points. Hopefully, this paper will stimulate such further experimental work. On the theoretical side, better approximations of the energy exchange terms of the model should be sought. To this end we are currently pursuing the idea mentioned at the end of Sec. II.

Even with the limitations and uncertainties that affect it, the simplified mathematical model that we have developed is of some interest. In the first place, it is the only model to date capable of describing the time-dependent behavior of thermoacoustic prime movers. Second, it can be used to compare design options. For example we have found that, under identical conditions in the stack, a device with a thicker cross section in the central part will develop a much stronger wave than one with a constant cross section.

Clearly, the present formulation can be extended in several directions. In the first place, we can account for heat conduction in the stack. Second, we can extend the model to the refrigerator case. Third, we can pursue the nonlinear aspects at the analytical level by using the techniques of weakly nonlinear stability theory. Efforts in all these directions are currently under way.

ACKNOWLEDGMENTS

Achard, J. L., and Lespinard, G. M. (**1981**). ''Structure of the transient wall-friction law in one-dimensional models of laminar pipe flows,'' J. Fluid Mech. **113**, 283–298.

Atchley, A. A. (**1992**). ''Standing wave analysis of a thermoacoustic prime mover below onset of self-oscillation,'' J. Acoust. Soc. Am. **92**, 2907–2914.

Atchley, A. A. (private communication).

Atchley, A. A. (**1994**). ''Analysis of the initial build-up of oscillations in a thermoacoustic prime mover,'' J. Acoust. Soc. Am. **95**, 1661–1664.

Atchley, A. A., Bass, H. E., and Hofler, T. J. (**1990**). ''Development of nonlinear waves in a thermoacoustic prime mover,'' in *Frontiers in Nonlinear Acoustics*, edited by M. F. Hamilton and D. T. Blackstock (Elsevier, New York), pp. 603–608.

Atchley, A. A., Hofler, T. J., Muzzerall, M. L., Kite, M. D., and Ao, C. (**1990b**). ''Acoustically generated temperature gradients in short plates,'' J. Acoust. Soc. Am. **88**, 251–263.

Fletcher, C. A. J. (**1988**). *Computational Techniques for Fluid Dynamics* (Springer-Verlag, Berlin).

Gaitan, D. F., and Atchley, A. A. (**1993**). ''Finite amplitude standing waves in harmonic and anharmonic tubes,'' J. Acoust. Soc. Am. **93**, 2489–2495.

Harten, A. (**1983**). ''High resolution schemes for hyperbolic conservation laws,'' J. Comput. Phys. **49**, 357–393.

Harten, A., and Osher, S. (**1987**). ''Uniformly high-order accurate nonoscillatory schemes. i,'' SIAM (Soc. Ind. Appl. Math.) J. Numer. Anal. **24**, 279–309.

Harten, A., Osher, S., Engquist, B., and Chakravarthy, R. (**1986**). ''Some results on uniformly high-order accurate essentially nonoscillatory schemes,'' Appl. Numer. Math. **2**, 347–377.

Osher, S. (**1984**). ''Riemann solvers, the entropy condition, and difference approximation,'' SIAM (Soc. Ind. Appl. Math.) J. Numer. Anal. **21**, 217–235.

Osher, S., and Chakravarthy, R. (**1984**). ''High resolution schemes and the entropy condition,'' SIAM (Soc. Ind. Appl. Math.) J. Numer. Anal. **21**, 955–984.

Pierce, A. D. (**1989**). *Acoustics* (American Institute of Physics, Woodbury), 2nd ed.

Press, W. H., Vetterling, W. T., Teukolsky, S. A., and Flannery, B. P. (**1992**). *Numerical Recipes in FORTRAN* (Cambridge U.P., Cambridge, England), 2nd ed.

Prosperetti, A., and Watanabe, M. (**1994**). ''Simplified model for the study of nonlinear processes in thermoacoustic engines,'' J. Acoust. Soc. Am. **96**, 3220.

Roe, P. L. (**1986**). ''Characteristic-based schemes for the euler equations,'' Annu. Rev. Fluid Mech. **18**, 337–365.

Rott, N. (**19xx**). ''Thermally driven acoustic oscillations, Part IV: Tubes with variable cross section,'' Z. Angew. Math. Phys. **27**, 197–224.

Rott, N. (**1980**). ''Thermoacoustics,'' Adv. Appl. Mech. **20**, 135–175.

Sod, G. A. (**1978**). ''A survey of several finite difference methods for systems of nonlinear hyperbolic conservation laws,'' J. Comput. Phys. **27**, 1–31.

Sweby, P. K. (**1984**). ''High resolution schemes using flux limiters for hyperbolic conservation laws,'' SIAM (Soc. Ind. Appl. Math.) J. Numer. Anal. **21**, 995–1011.

Swift, G. W. (**1988**). ''Thermoacoustic engines,'' J. Acoust. Soc. Am. **84**, 1145–1180.

Swift, G. W. (**1992**). ''Analysis and performance of a large thermoacoustic engine,'' J. Acoust. Soc. Am. **92**, 1551–1563.

Watanabe, M., Prosperetti, A., and Yuan, H. (**1997**). ''A simplified model for linear and nonlinear processes in thermoacoustic prime movers. Part I. Model and linear theory,'' J. Acoust. Soc. Am. **102**, 3484–3496.

Wheatley, J. (**1986**). ''Intrinsically irreversible or natural heat engines,'' in *Frontiers in Physical Acoustics*, edited by D. Sette (North-Holland, Amsterdam), pp. 35–475.